Acta Materialia 213 (2021) 116951

Contents lists available at ScienceDirect

Acta Materialia

journal homepage: www.elsevier.com/locate/actamat

Simulations of primary damage in a High Entropy Alloy: Probing enhanced radiation resistance

O.R. Deluigi[a,b], R.C. Pasianot[a,c,d], F.J. Valencia[e,f], A. Caro[g], D. Farkas[h], E.M. Bringa[a,b,i,*]

[a] CONICET, Mendoza, Argentina
[b] Facultad de Ingeniería, Universidad de Mendoza, Mendoza, 5500, Argentina
[c] Instituto Sabato UNSAM/CNEA, Argentina
[d] Gerencia de Materiales, CNEA, Av. Gral. Paz 1499, San Martín, Argentina
[e] Centro de Investigación DAiTA Lab, Facultad de Estudios Interdisciplinarios, Universidad Mayor, Santiago, Chile
[f] CEDENNA, Universidad de Santiago de Chile, USACH, Av. Ecuador 3493, Santiago, Chile
[g] College of Professional Studies, George Washington University, Ashburn, Virginia 20147, USA
[h] Department of Materials Science and Engineering, Virginia Polytechnic Institute and State University, Blacksburg, VA 24061, USA
[i] Centro de Nanotecnología Aplicada, Facultad de Ciencias, Universidad Mayor, Chile

ARTICLE INFO

Article history:
Received 6 April 2021
Accepted 28 April 2021
Available online 6 May 2021

Keywords:
Irradiation defects
Molecular dynamics
High-entropy alloy
Primary knock-on atom

ABSTRACT

High Entropy Alloys (HEA) attract attention as possible radiation resistant materials, a feature observed in some experiments that has been attributed to several unique properties of HEA, in particular to the disorder-induced reduced thermal conductivity and to the peculiar defect properties originating from the chemical complexity. To explore the origin of such behavior we study the early stages (less than 0.1 ns), of radiation damage response of a HEA using molecular dynamics simulations of collision cascades induced by primary knock-on atoms (PKA) with 10, 20 and 40 keV, at room temperature, on an idealized model equiatomic quinary fcc FeNiCrCoCu alloy, the corresponding "Average Atom" (AA) material, and on pure Ni. We include accurate corrections to describe short-range atomic interactions during the cascade. In all cases the average number of defects in the HEA is lower than for pure Ni, which has been previously used to help claiming that HEA is radiation resistant. However, simulated defect evolution during primary damage, including the number of surviving Frenkel Pairs, and the defect cluster size distributions are nearly the same in all cases, within our statistical uncertainty. The number of surviving FP in the alloy is predicted fairly well by analytical models of defect production in pure materials. All of this indicates that the origin of radiation resistance in HEAs as observed in experiments may not be related to a reduction in primary damage due to chemical disorder, but is probably caused by longer-time defect evolution.

1. Introduction

Different kinds of materials such as metallic alloys, ceramics, polymers, and composites are irradiated in different scenarios, some with technological relevance, as in nuclear reactors [1]. Here fast neutrons transfer kinetic energy to atoms in the structural material and create a primary knock-on atom (PKA). PKAs generate a cascade of collisions that causes damage to the material, such as creation of pairs of interstitials and vacancies, i.e. Frenkel Pairs (FP) [2,3], which can cluster and lead to dislocation loops and amorphous zones [3,4].

High Entropy Alloys (HEAs) show excellent mechanical properties, such as high strength and wear resistance [5–9]. HEAs with face-centered-cubic structure (fcc) present a remarkable thermo-mechanical behavior [8,10,11] which can be useful in radiation environments. In this context, several experimental studies have shown radiation resistance for fcc [12–16] and body-centered-cubic (bcc) [17] HEAs, as well as High Entropy ceramics [18].

Theoretical arguments addressing this behavior points towards several properties that are distinctive of HEA. Among them, the anomalous energy and mass transport in concentrated solid solutions. In fact, the energy deposited during a collisional phase of a cascade in metallic HEA is carried away by electrons and phonons, which have been shown to be significantly less efficient than in conventional alloys [13–15,19]; as a result, the thermal phase of the cascade is expected to last longer [20], favoring recombination. For mass transport, the rugged energy landscape resulting from

* Corresponding author at: Facultad de Ingeniería, Universidad de Mendoza, Mendoza, 5500, Argentina.
E-mail address: ebringa@yahoo.com (E.M. Bringa).

https://doi.org/10.1016/j.actamat.2021.116951
1359-6454/

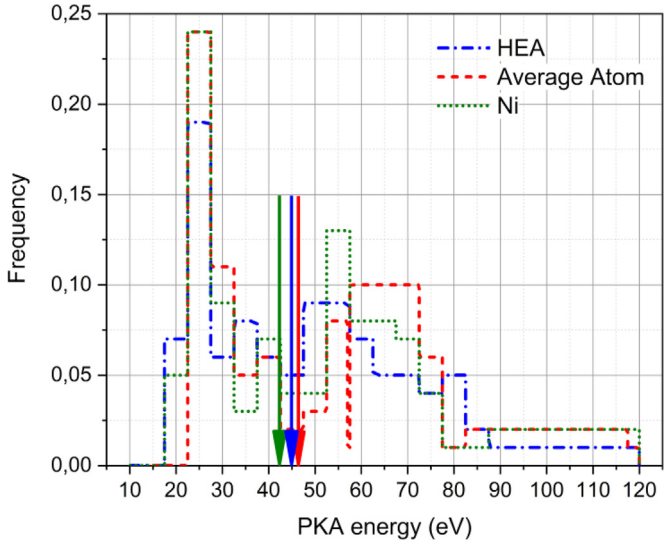

Fig. 1. Displacement energy distribution. Dash-dot lines (blue) correspond to HEA potential, short-dash lines (red) to Average Atom, and dot lines (green) correspond to pure Ni, using the corresponding HEA potential. Arrows indicate average values for each potential. Displacement energy distributions are calculated on the basis of 100 random directions for all cases, increasing the energy of the PKA in steps of 5 eV (For interpretation of the references to color in this figure legend, the reader is referred to the web version of this article.).

the different electronic structure and mass of the constituents, alongside other effects, translates into anomalous diffusion [21–24], trapping, and binding [15], also impacting dislocation motion [25,26]. Testing each one of these mechanisms has been the focus of research in recent times.

Molecular Dynamics (MD) simulations have been extensively used to study PKAs in different materials [2,4,27–31], mostly in single elements, or in single elements with impurities. Recently, thanks to improved interatomic potentials, there have been a number of MD studies of PKAs in binary alloys [13,32–39], ternary alloys [35,38–41], and quaternary alloys [20,42]. There are simulation studies of cumulative damage by 5 keV PKAs in concentrated solid solution alloys (CSSA) [35,41] showing larger damage in the alloy than in Ni at low dose. However, recent results for single PKA simulations at larger PKA energy in binary [36] and medium entropy alloys [20] indicate a larger number of defects in Ni than in the alloys, which has been related to alloy radiation resistance.

Despite this growing number of simulations about radiation damage in alloys, there are only few radiation damage MD simulations of HEA, containing at least 5 or more elements as in the criteria by Miracle and Senkov [5]. All of these simulations are for fcc CoNiCrFeMn, for 10 keV single PKA [43], cumulative 3 keV PKA [44], and surface bombardment at 700 K with 3 keV [45]. They point to several possible reasons for radiation resistance, when comparing HEA to pure Ni: recombination ratio of Frenkel Pairs is higher for the HEA, and defect clusters seem to be less stable during thermal annealing [43]. The latter simulations, however, were carried out without including a proper description for the short range behavior of atom-atom interactions, the ZBL potential [46], resulting in an uncontrolled scattering cross-section for energetic collisions, and thus casting doubts about the validity of the results.

Computer simulations of radiation damage in HEAs face the challenge of adequately describing the complex and varied responses of those alloys. Models have recently been used where alloy components are represented by a single artificial potential. One of these models is so called “Average Atom” (AA) [47–49], where elastic and plastic properties are similar to average values for the HEA, but where radiation-induced defects could behave differently

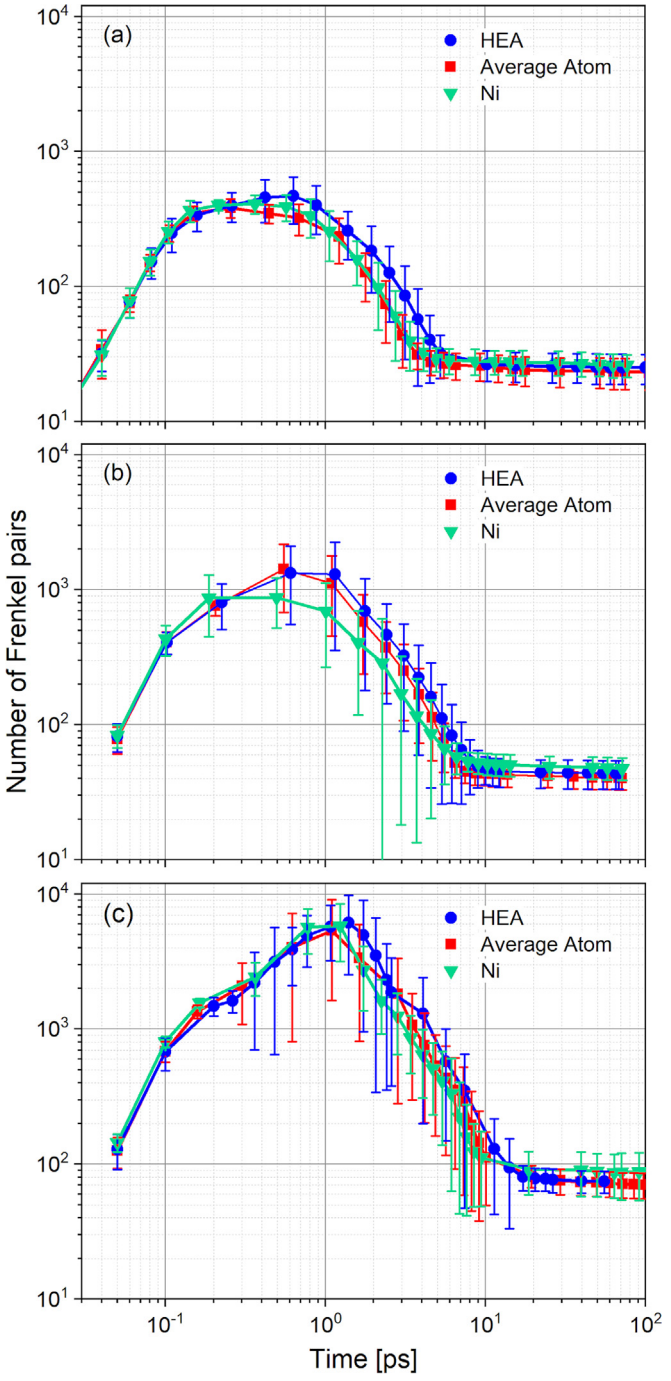

Fig. 2. Average number of Frenkel pairs for all cascade simulations with (a) 10 keV (b) 20 keV and (c) 40 keV PKA energy, for Average Atom (red squares), HEA (blue circles) and pure Ni (green triangle). For 20 keV simulations HEA the peak damage state occurs after 0.60 ps, after 0.549 ps for AA and 0.49 for Ni. Error bars indicate standard deviation after averaging over all cascades for each case. Also in (c), for some of the AA simulations the peak occurs approximately 1 ps later, which results in a high standard deviation near 3 ps (For interpretation of the references to color in this figure legend, the reader is referred to the web version of this article.).

than in the HEAs. Regarding the alloy itself, the aim of the current potentials is not accuracy but rather to be a tool to study trends of significant alloy properties [50].

In the present work, using MD simulations we carried out collision cascade simulations in an equiatomic FeNiCrCoCu HEA, and compared our results to the corresponding AA material. We run PKAs with 10 keV, 20 keV and 40 keV, at room temperature. The

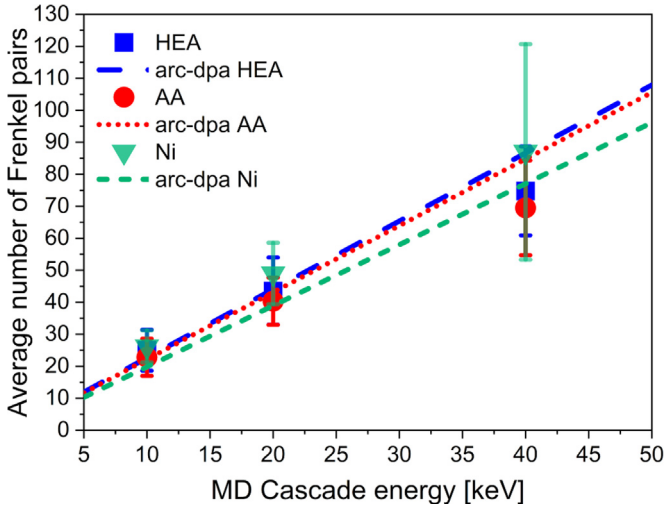

Fig. 3. Average number of surviving Frenkel pairs for all samples compared with the analytical ARC-DPA model developed by Nordlund and co-workers [3].

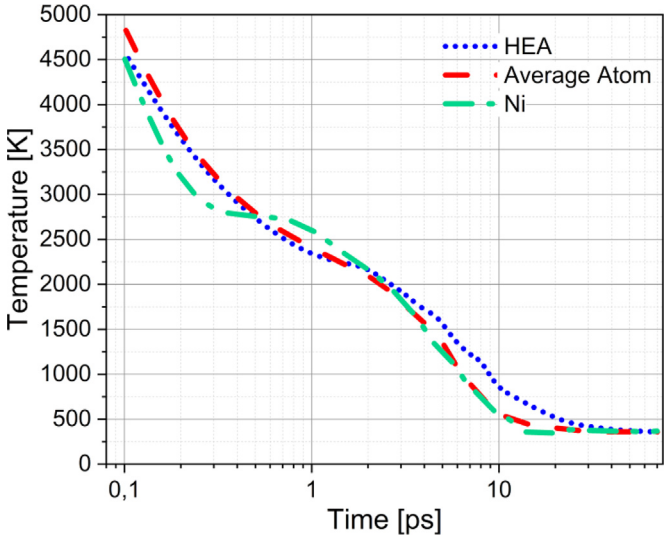

Fig. 4. The average temperature at the core of the cascade in 3 samples of HEA, Average Atom and pure Ni during the simulations time for E_{PKA}= 20 keV.

PKA energies in our simulations are higher than in previous studies [43,44] in order to obtain a larger number of primary defects, while staying in a regime without significant cascade splitting or sub-cascades. We report defect generation and evolution for both materials and, in some cases, compare with pure Ni.

2. Methods

Molecular Dynamics (MD) simulations were carried out to study primary irradiation damage of a High Entropy Alloy composed by Fe, Ni, Cr, Co and Cu. The sample is equiatomic, i.e. contains the same number of atoms for each atom type. This is an fcc alloy with lattice parameter a_0 = 0.352 nm. The atomic interaction was modeled using a recently developed EAM (Embedded Atom Method), as reported by Farkas and Caro [50]. It is important to realize that these are 'toy models', in the sense that we can expect only some properties to be well described, such as metallic radius, the heat of mixing of the binary alloys, the fcc phase stability with respect to hexagonal closed-packed (hcp) and bcc, the scattering cross sections of the elements, and the lattice parameter. We also use an AA potential, derived from the alloy potential using 20% concentration for all the five elements [47], as in the present HEA sample. Properties for both HEA and AA potentials are included in the Supplementary Material, Table S1. For this work, all potentials also feature a spline to short-range ZBL interactions [46], which are key in radiation damage simulations. The ZBL potential was smoothly splined to the EAM pair potential for distances between 0.1 nm and 0.2 nm, as is customarily done in the literature. This procedure does not affect the equilibrium properties. The same method was used for all potentials, and it gives reasonable values for displacement energies of the pure metals, tabulated for instance in [3]. Embedding energy contributions for these potentials are not significant below 0.2 nm. A detailed description of the potentials is included in the Supplementary Material. As an example, Fig. S1(a) plots the AA potential with and without the spline to ZBL. Moreover, Fig. S1(b) shows pair potential shapes in a critical region for FP generation; there one sees that no artifacts are introduced because of the match to the ZBL potential, thus comparisons among the different potentials should be valid.

Our simulations were carried out with the LAMMPS package [51] and the resulting samples were visualized and analyzed with OVITO and its included tools [52–54]. Structure analysis was carried out using "Polyhedral template matching" (PTM) [55], with a RSMD=0.2. For some cases we used Common Neighbor analysis (CNA). Dislocations were analyzed using 'Dislocation eXtraction Algorithm (DXA) [53]. Vacancies and interstitials were analyzed with Wigner–Seitz cell analysis. Number and size of clusters were computed using the Cluster Analysis tool from OVITO.

All simulations used a cubic box with $L_x = L_y = L_z = 64a_0$, all along canonical axes, containing 1,048,576 atoms. For all simulations we employed periodic boundary conditions (PBC). The samples were first subjected to an energy minimization and box relaxation, to achieve zero initial stress, then subjected to 300 K thermostat and a zero pressure barostat, during 10 ps. To initialize the cascade we select an atom near the origin of the sample, from any of the elements of the alloy (Fe, Ni, Cr, Co and Cu), and then set a primary knock-on atom (PKA) energy of 10, 20 and 40 keV, with a random PKA velocity direction. Cascade evolution was followed with a variable time step using a microcanonical ensemble (NVE).

There are several methods to include electronic stopping losses in cascade simulations [56–60]. One of the computationally efficient methods is to include a friction force, with damping parameter γ, for all atoms with more than a threshold kinetic energy, and this is used in all simulations presented here, for a threshold of 10 eV [40]. We are not aware of experimental measurements of electronic stopping in such a HEA, and ab-initio modeling has been carried out only for some binary alloys [61]. Damping was calculated with a linear fit to electronic stopping power S_e eV Å $[^{-1}]$ as a function of ion velocity v Å $[ps^{-1}]$, such that$\gamma = S_e/v$, with S_e values obtained from SRIM [62]. For the HEA the damping parameter was obtained as the average of all damping parameters for self-ion stopping, shown in Table SII, giving γ=0.005 eV/ps Å $^{-2}$. This is similar to Bragg's additive rule [63].

For statistical purposes we have carried out tens of cascades for each case. In HEA, there were 50 cascades for 10 keV, 50 cascades for 20 keV, and 25 cascades for 40 keV, choosing with the same probability atoms of each type as the initial PKA. In AA, there were 10 cascades for 10 keV, 25 cascades for 20 keV, and 15 cascades for 40 keV. For Ni, we use the same number of cascades as in AA. The parameters for these simulations are the same as for the HEA case.

Because of its potential relevance for the collisional thermal spike stage, we have estimated the melting temperature of the HEA, AA and Ni, to be 2260 K, 2340 K, and 2340 K, respectively. These estimates were obtained as follows: a box, with 216,000 atoms, was kept at zero pressure and heated in steps of 10 K, maintaining temperature constant during 200 ps before the next increase. Monitoring the potential energy of the system showed

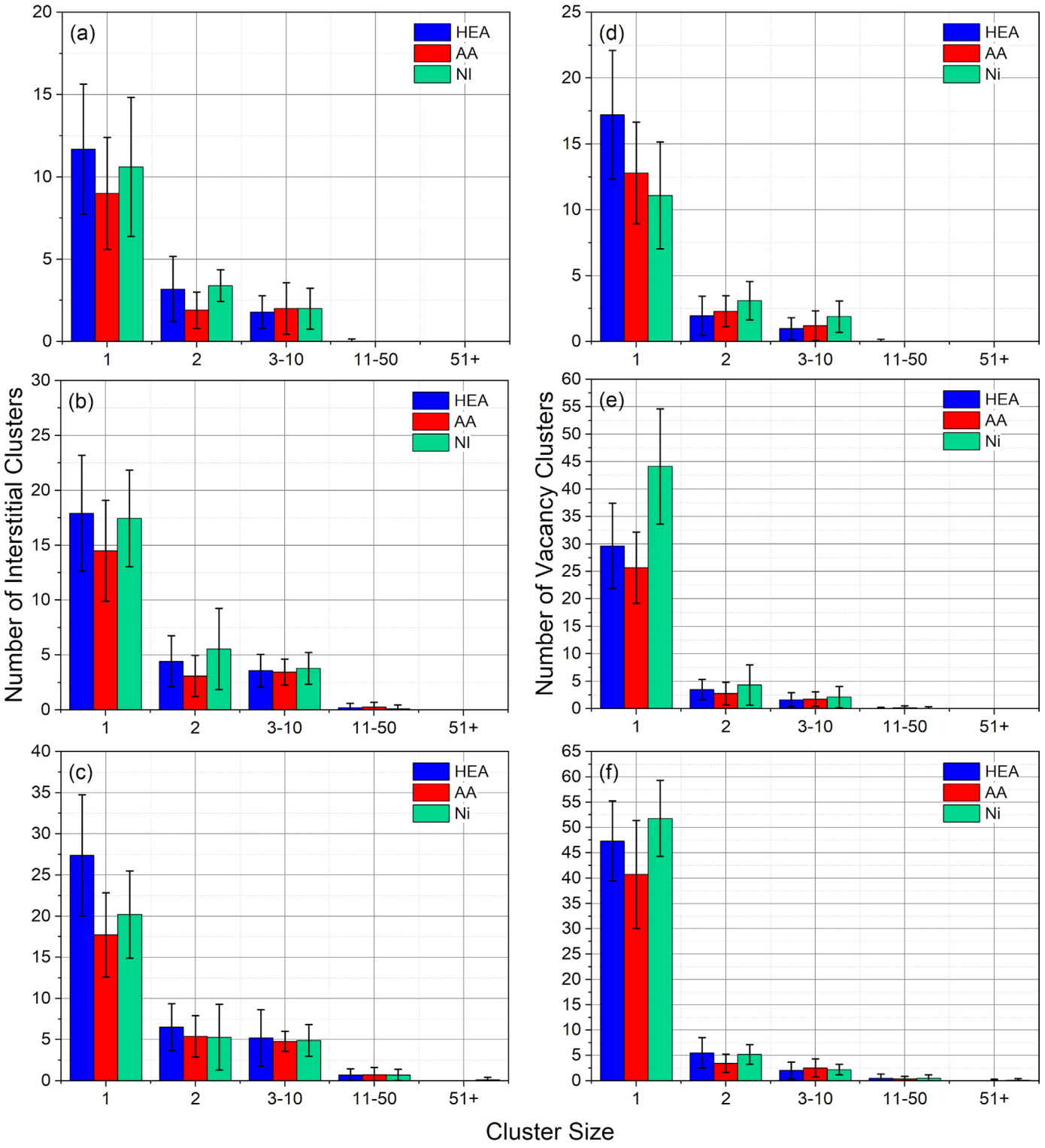

Fig. 5. Average number of interstitials and vacancies clusters in cluster size distributions for HEA, AA and pure Ni, after (a) and (d) 10 keV, (b) and (e) 20 keV and (c) and (f) 40 keV after PKA simulations.

a sudden jump of nearly 0.2 eV at a certain temperature, which was taken as the melting temperature. Melting was verified by inspection of the pair-correlation function, g(r), and possible structure identification with PTM, using OVITO. This approach neglects overheating effects but provides a reasonable value of melting temperature. The final temperature of our simulations (HEA and Average Atom) after a PKA collision cascade was around 335 K for 10 keV, 360 K for 20 keV, and 430 K for 40 keV PKAs, confirming that our systems are large enough to successfully dissipate the energy of the cascade, considering that electronic stopping is included.

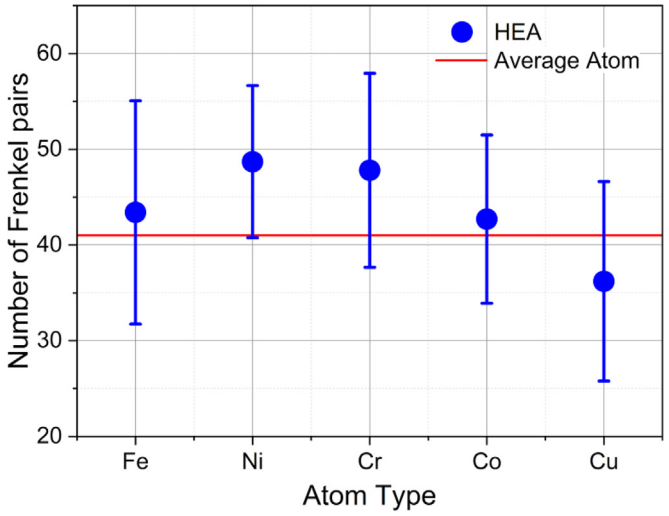

Fig. 6. Average number of Frenkel Pairs for all HEA cascade simulations, starting with a PKA of certain atom type compared with the average obtained with Average Atom.

Table 1
Comparison of defect formation energies between HEA and "Average Atom".

	Fe	Ni	Cr	Co	Cu	AA
$E_{Dumbbell}$ (eV)	5.32	4.95	4.85	5.11	4.82	5.02
$E_{Crowdion}$ (eV)	———-	———-	———-	———-	———-	5.44

3. Results and discussion

Using the AA potential we have estimated the vacancy formation energy for the HEA, as well as the interstitial formation energy for every single species. The former amounts to 1.42 eV, while the latter are reported in Table 1, including those for the AA itself. Figures represent thermodynamic average values. Stable interstitials are of the <100> dumbbell type, and octahedral interstitials decay to dumbbells, while <110> crowdions (centered in $(1/4,1/4,0)a_0$) have higher formation energy. Mean values are similar to the values for AA, as shown in Table 1. As expected, defect formation energies in the HEA have variations due to compositional fluctuations.

Average displacement energies (E_d) were calculated using a simulation cell with $(18 \times 18 \times 18)a_0{}^3$=23328 atoms, at T=0 K, for 100 PKAs in random directions. E_d values of 45 (+-2) eV and 46 (+-2) eV are obtained for the HEA and the AA, respectively. Both distributions are extremely wide, as shown in Fig. 1, going from 15 eV up to more than 100 eV, as expected from an fcc material. The E_d for pure Ni using our HEA potential is 43.4 (+-1.9) eV, similar to the values obtained for HEA and Average Atom, as also shown in Fig. 1 (see Supplementary Material Table S3). Other Ni potentials give similar results, for instance Ed=39 eV is reported in [3].

As advanced above, in order to study possible modifications in primary damage at different PKA energies, we performed cascade simulations using 10, 20 and 40 keV PKAs, for HEA, AA and pure Ni, and there were no differences in primary damage within the uncertainties in the study, as shown in detail below.

Fig. 2 shows the time evolution of average and standard deviation of Frenkel pairs produced by collision cascade for all simulations (HEA, AA, and Ni) at PKAs of 10, 20 and 40 keV. Here we can see that the production of defects is very similar in HEA and AA, and fairly similar to Ni, although there is a slight trend for the HEA case to decay somewhat slower than Ni. In the early, ballistic, stage of collision cascades a large number of defects are produced, with a maximum occurring near 1 ps. Most FPs recombine during the following stage and, after approximately 10 ps the number of FPs has reached a steady, final value, a couple orders of magnitude lower than the peak value. This comparison between Ni and the HEA, is consistent with results for irradiation of a quaternary alloy [20].

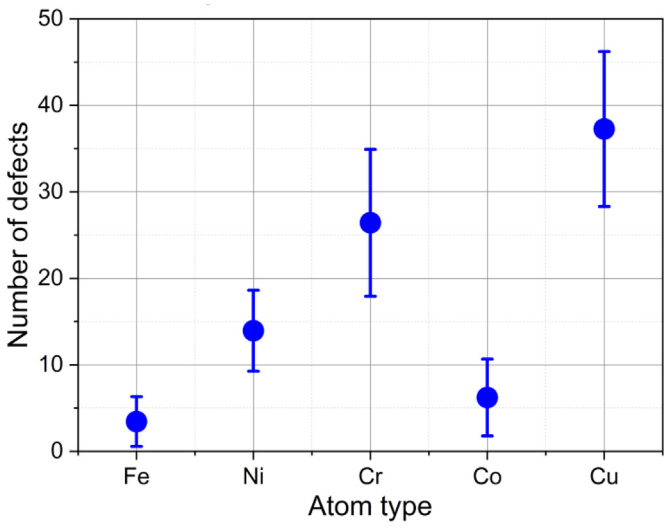

Fig. 7. Average number of defects of a given type. Their sum gives 87, i.e. the total number of vacancies plus interstitials for these cascades (43.5 Frenkel pairs approximately). Most defects are due to displaced Cu atoms, and Fe atoms have the smaller contribution to defect production.

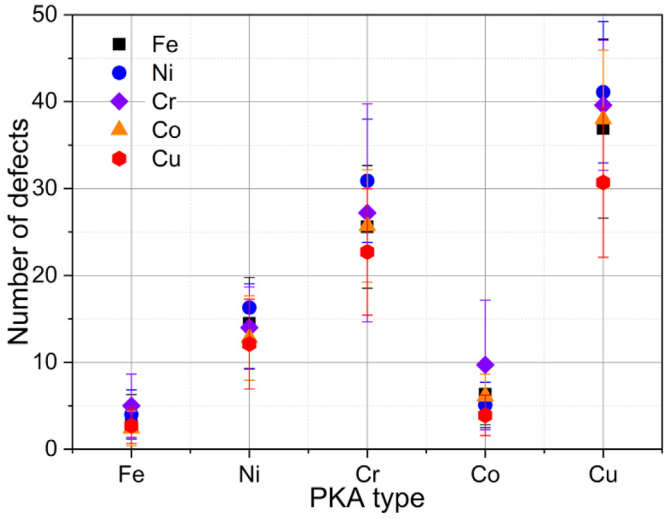

Fig. 8. Same as Fig. 7, but now discriminating by PKA type.

The mean value of FPs in the HEA for 20 keV is slightly higher than in the AA during the recombination phase. From Fig. 2, recombination rate can be calculated using the equation: $n = \frac{FP_{MAX} - FP_S}{FP_{MAX}} * 100$. Here FP_{MAX} corresponds to the peak number of FPs, and FP_S is the number of surviving FPs at the end of each simulation. Fig. S2 in the SM shows recombination rates for all of our simulations, giving values of 94–99%. Such high recombination rates are also found for quaternary alloys [20]. Surviving FPs and recombination rates can be considered identical for HEA and AA 20 keV cascades. Despite a sometimes lower number of maximum displacements, Ni shows a lower mean recombination rate, which leads to more surviving FPs at the end of primary damage. However, recombination rates for Ni are the same that in HEA and AA within our statistical uncertainty. Understanding of detailed radiation response would benefit from calculation of recombination ra-

dius of the HEA for isolated FPs, similarly to what was done for a FeCrNi [64]. However, the simulations we have carried out suggest that the effective recombination radius after an energetic cascade would be similar in HEA and AA materials, contradicting those results for single FPs in FeCrNi.

To analyze the results obtained from the collision cascade simulations, we plot in Fig. 3 the average number of Frenkel pairs that survived the final stage of the cascade for all simulations (70 ps). We note that FP production is heavily potential dependent [65]. For pure Ni, different potentials can give different values, with a MEAM potential [20] giving reasonable agreement with our result, considering error bars. From our simulations, it is clear that, within the statistical error in our simulations, the number of surviving FP is the same for HEA, AA and Ni. In all cases FP production mean values are higher for Ni than in our HEA sample, for similar displacement energies. Comparison of FP production between HEA and a single element like Ni could then lead to the belief that HEA are per se radiation resistant due to chemical complexity, but results for the AA disprove this particular conclusion.

The original version of our potential has been recently used to build and irradiate the quaternary FeNiCrCo alloy [66]. Though their emphasis is on the simulation of cascades near grain boundaries, they observe Frenkel pair production for cascades in standard bulk conditions that is lower than our results for the quinary FeNiCrCoCu, especially for the 20 keV PKA case. The differences may be due to the different composition used, or to a different procedure in handling the short-range corrections. These corrections are calculated using LAMMP's overlay feature, where multiple potentials are added to compute the interaction between atoms, which can be problematic for heavy atom collisions.

We also compare the average numbers of surviving FPs from HEA simulation with values obtained using the NRT model: $FP_{NRT} = 0.8\ T_d/(2\ E_d)$[2,67], as shown in Table S4 of Supplementary Material. Here FP_{NRT}represents the number of surviving FPs, T_d is the damage energy, and E_d the average displacement energy. T_d is the kinetic energy available for creating atomic displacements, which is smaller than E_{PKA}, the initial PKA energy, due to electronic energy loss. In our simulations, using stopping friction γ=0.005 eV/ps Å $^{-2}$ leads to $T_d \sim 0.9E_{PKA}$. The role of electronic loss is complex, but in simple models it re-scales the available damage energy and, therefore, would only shift the effective PKA energy. We also compare damage production with a model developed recently by Nordlund and co-workers [3], the Athermal Recombination Corrected Displacements Per Atom (arc-dpa), which corrects NRT with a pre-factor, requiring two parameters (b and c) from experiments or simulations:$N_{ARC-DPA} = \varepsilon(T_d)\ FP_{NRT}$, where $\varepsilon(T_d) = [(1-c)/(2\ E_d/0.8)^b]\ T_d^b + c$. For our estimates in Fig. 3 and Table S4, we have taken the average values for these two parameters for Cr (b=−1, c=0.37) [68] and Cu (b=−0.68, c=0.16) [3], which are the most frequent recoils at the recombination phase of the HEA. For pure Ni, b=−1.01 and c=0.23 [3]. For the NRT and ARC-DPA calculation, Td=0.9E_{PKA}. The resulting ARC-DPA values agree within 1%-30% with our MD simulations, which is reasonable given that the parameters were obtained from fits using simulations with other interatomic potentials. This model estimations disregard alloying effects, and this agreement also indicates that, according to primary damage, there is no clear radiation resistance in the HEA studied here, compared to pure materials.

The number of FP in HEA and AA are equivalent, but Ni shows more FPs, in agreement with previous related studies [20,43]. Ni has a similar melting temperature, but higher phonon heat conductivity [19,34]. This leads to a faster temperature decrease at the core of the cascade, which reduces recombination, as reported above for the recombination rates. Typical temperature evolution cases for 20 keV are shown in Fig. 4. For a given PKA, the center of the cascade was selected as the center of mass of atoms with more than 10 eV, at 0.1 ps. A sphere of radius 2.5 nm, centered at that position, was considered for all subsequent times, and temperature was calculated in that sphere, still filtering out atoms with less than 10 eV, resulting in the values shown in Fig. 4. That sphere contained around 5000 atoms at 0.1 ps. Note that HEA and AA have similar cooling rates during the early ballistic stage, but after a few ps, AA cools slightly faster. Due to disorder, HEA is expected to have lower phonon heat conductivity than AA, possibly explaining this late difference.

Temperature profiles for 10 keV and 40 keV appear similar to the ones shown for 20 keV. The lower heat conductivity of the HEA was proposed to be one of the reasons for the radiation resistance of HEAs [13,19], and in simulations of damage in a quaternary alloy, when compared to pure Ni [20]. However, this thermal conductivity difference might not be large enough to ensure significant differences in defect production and survival during primary damage.

HEA and AA results are the same not only in the same total number of FP, but also in how they are clustered. To describe the size and number of interstitials and vacancies clusters we calculated the average and standard deviations for all samples. In Fig. 5 we observe interstitial and vacancy cluster size distributions for HEA, Average Atom and pure Ni. Regarding interstitials in Fig. 5(a–c), clusters of 1-2 intesticials are the most abundant for the three cases, as expected. For 20 keV PKAs, the largest interstitial clusters contain 17 atoms for HEA, and 20 atoms for AA. Cumulative simulations at 5 keV display larger defect clusters in Ni than in alloys [34,41]. There is some evidence that this could also occur for single PKAs in binary alloys [36] and in medium entropy alloys [20]. Our simulations are not conclusive on this, and a significantly larger number of cascades would have to be simulated to obtain reliable statistics for the formation of large defect clusters during primary damage. For cascades in a quaternary alloy [20], some large loops (more than 50 interstitials) were found for PKA with 30 keV and above. We do not find such large clusters in the HEA simulated here. Vacancy cluster size distributions are shown in Fig. 5(d–e). We observe that AA and Ni are prone to produce larger vacancy clusters than HEA. However, as for large interstitial clusters, more statistics would be needed to confirm significant differences between HEA and AA regarding large vacancy cluster production. In order to better understand the primary damage results, we present below a more comprehensive analysis for 20 keV cascades. In Fig. 6 we compare the average number of FPs obtained in the HEA for PKAs of different atom types, and for the AA. Taking into account error bars, there is no difference in defect production. Cu PKAs give the lowest mean value of FPs. The most common type of defect for the HEA corresponds to displaced Cu atoms while the least common are Fe atoms as shown in Fig. 7, following the expected (anti)correlation with dumbbell formation energies reported in Table 1. Furthermore, it can be said that this trend in the number of defects is maintained regardless of the type of PKA, as shown in Fig. 8.

A few cascade simulations in HEA and AA resulted in dislocation loops, which were more frequent in AA. The Peierls barriers are much lower in AA [47], and this might influence loop size. Fig. 9 presents snapshots from HEA and AA simulations for 20 keV PKA. These are not randomly selected, but the cascades with the largest surviving interstitial clusters in each case. From Fig. 9(a) and (d) it can be seen that the cascade core is compact and it has not split into sub-cascades. Fig. 9(b) and (e) show the final configuration of defects, including mostly point defects. Fig. **9(c)** and **9(f)** show sites associated with vacancies and interstitials, identified by Wigner-Seitz analysis. Dislocations identified with DXA are also shown. Some interstitials form stacking faults (SFs), which appear as hexagonal closed-packed (hcp) atoms. Some small twin platelets can also be identified using an alternative tool, the Crystal

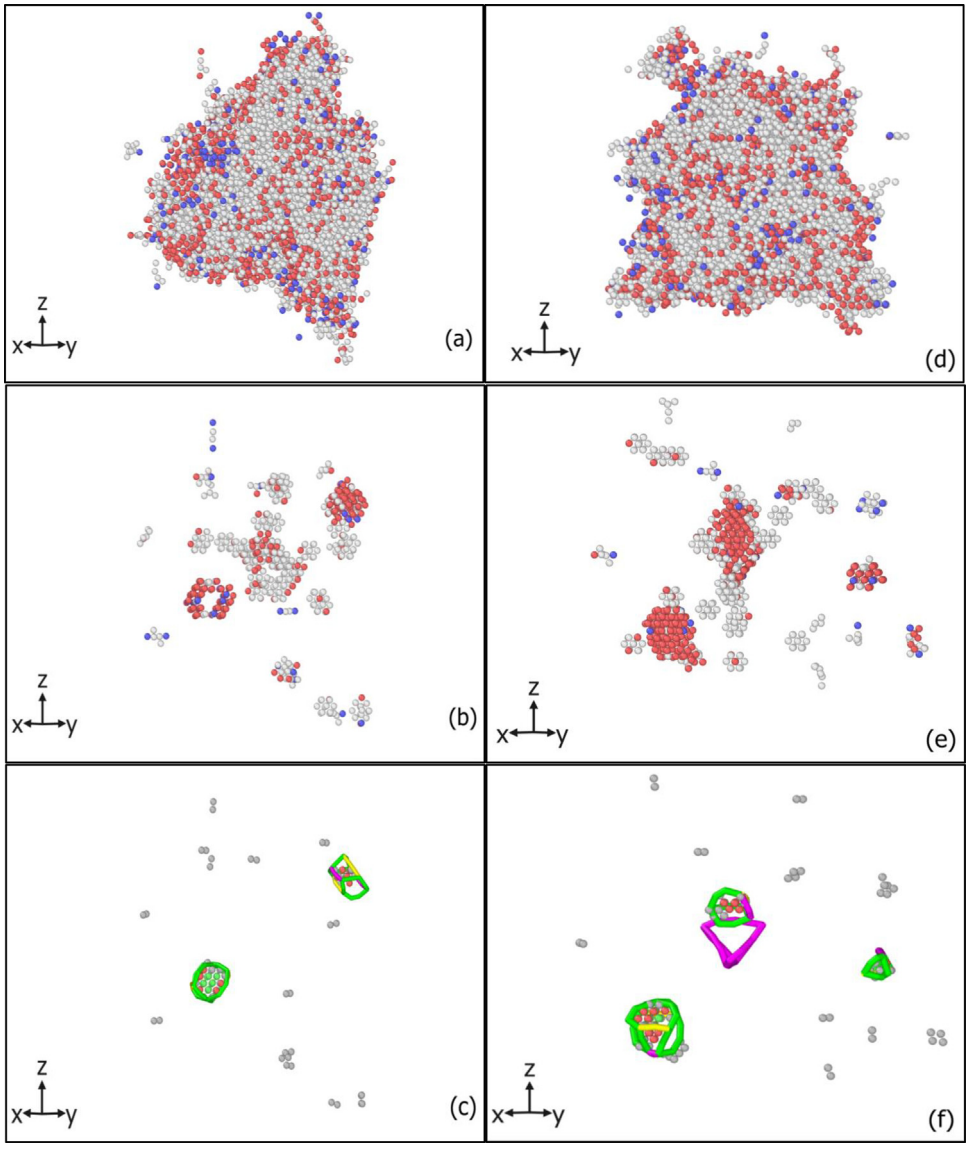

Fig. 9. Defects after a single 20 keV PKA. (a)-(c) HEA (Fe PKA). (d)-(f) Average Atom. All fcc atoms have been removed from frames (a),(d). Structure type given by PTM (rmsd=0.2) from OVITO. Atoms are colored according to their structure: hcp (red), fcc (green), and unknown (white). (a) and (d) are close to the defect generation peak. (b) and (e) show the final configuration. (c) and (f) show dislocations identified by DXA from OVITO. Wigner-Seitz occupation from OVITO has been used to filter-out all sites with occupation 1. Dislocations coloring according to dislocation type: (⅓)<111> Frank partials (light blue), (⅓)<100> Hirth partials (yellow), (⅙)<112> Shockley partials (green), and (⅙)<110> Stair-rod partials (purple). Stacking faults associated with partial dislocations appear as hcp atoms. Several interstitial dumbbells can be seen in (c) and (f) (For interpretation of the references to color in this figure legend, the reader is referred to the web version of this article.).

Analysis Tool (CAT) [52,53]. The presence of SFs is expected in fcc materials with relatively low SF energy, as it is the case for both HEA and AA (see Supplementary Material Table 1). In Fig. 9(c) for the HEA, most dumbbells are pure Cu, as expected. There are some mixed dumbbells with Cu, Cr or Ni. Fe and Co, which give rise to the least number of defects, do not participate in stable dumbbells at the end of the primary damage stage.

Fig. 9 shows some differences in defect morphologies between the AA and the HEA models, even though the number of FPs and the clustered fraction are nearly the same. For instance, the more frequent dislocations in AA include sessile loops like stair-rod dislocations, and this difference can therefore affect the long term evolution of the system.

Snapshots similar to the ones in Fig. 9, but for 10 keV and 40 keV PKA are shown in Supplementary Material Figs. S3 and S4. Snapshots for Ni cascades are shown in Figs. S5–S7. Even at the relatively high energy of 40 keV, simulated cascades are also compact and generally do not show splitting, as in the cascade core in Fig. S4(a) and (d), and in S7(a). Irradiated Ni alloys can display complex dislocation arrays, with 1/6<112> partial dislocations and 1/2<110> dislocations [20], also observed in this study. In Figs. S3 and S4 we observe some stacking faults parallelepipeds, as for high energy PKA in a NiCoCrFe alloy, using a different potential [20]. We also observe short segments of sessile Hirth dislocations for both HEA and AA, which would have negligible mobility as mentioned above for stair-rod dislocations. In Fig. S7 we observe some complex defect structures for 40 keV cascades in Ni, as in Ref. [20] for 50 keV cascades.

Essentially no interstitial loops but only small defect clusters were observed in the 10 keV cascades performed by Do and Lee [43] in CoNiCrFeMn. This was the case even after annealing at 773 K during 15 ns. From this and by comparison with similar simulations in pure Ni, they argued that interstitial clusters in the HEA are relatively unstable, which would confer some radiation resis-

tance. In contrast, our cascades do contain interstitial loops, albeit small for 10 keV. Moreover, we have carried out 2 ns annealings at 1650 K for the cascades in Fig. 9. The HEA case also shows clear 1D migration of large interstitial clusters, without significant reduction in cluster size or dislocations length (see Supplementary Material Fig. S8(a)). The AA case shows clear 1D migration of large interstitial clusters, without significant reduction in cluster size, as expected in pure fcc materials (see Supplementary Material Fig. S8(b)). Migration of interstitial clusters in alloys is an active field of research, with some MD simulations for binary alloys showing 3D migration [69], while there is experimental evidence for 1D migration even in quaternary alloys [26], with the added possibility of cluster stability playing a role in migration [70].

4. Summary and conclusions

There is some experimental evidence of radiation resistance in HEAs [12–17,41], and MD irradiation simulations of an fcc HEA with 10 keV PKAs, at 776 K, were used to support this evidence [43]. A higher point-defect recombination was found in the HEA compared to pure metals, and it was argued that larger defect clusters were less stable, leading to possible long-term cluster dissolution and radiation resistance, when compared to pure Ni [43]. However, those simulations were carried out without a ZBL potential for energetic collisions, and would need to be taken with caution.

In this work, we aim to separate the effect of having a random alloy, from the effect of different material properties, and that is why we focus our comparison to results using an fcc equiatomic alloy, FeNiCrCoCu, and an “Average Atom” (AA) material, instead of comparing to pure Ni [14,20,43,66]. In general, in order to truly assess radiation resistance due to chemical complexity in HEA, it can be considered that the most meaningful comparison for simulated primary damage would be with an AA potential that corresponds to the HEA potential used, as opposed to comparisons with pure Ni, or with alloys of different compositions. This comparison appears as the ideal way to isolate the effects of complexity, separating it from the effects that other details of the potential may introduce. This perspective can be beneficial and will hopefully help with the interpretation of current experimental results, understanding what the effect of chemical complexity is, separately from the many other possible effects.

Frenkel pair production in the HEA is certainly lower than in pure Ni. However, the fact that Frenkel pair production is the same for the AA material means that the disorder in the HEA does not guarantee enhanced radiation resistance. Actually, FP production is reasonably well reproduced by the ARC-DPA model prediction [3], which has been validated for multiple single-element materials, but does not include alloying effects.

We find no significant differences between the HEA and the AA material in our simulations of primary damage, but they could appear at a later stage, or due to cumulative bombardment, which might enhance temperature-related effects. Another factor which might also lead to differences in primary damage is significant cascade splitting [29,71] at much higher PKA energies, above 50 keV. This is only speculation, considering that subcascades might interact differently in pure Ni or AA versus HEA, since heat transport between subcascades would be significantly lower in the HEA [13,40]. Regarding dose effects, Beland and co-workers showed that there were fewer radiation-induced defects in FeNi than in Ni at low dose, but the opposite occurred at high dose [34]. Zhang and co-workers also showed the same for other binary alloys [14].

Experiments and simulations for single-phase concentrated solid solution alloys (SP-CSAs) display unique radiation-induced microstructure, and SP-CSAs including Ni, Co, Fe and Cr, showed Ni segregation even at relatively low irradiation dose [41]. Something similar happens for a bcc 4-component alloy [17], where point defect mobility is suggested to be the reason for exceptional radiation tolerance. If vacancies and interstitials have similar mobility a large recombination would be achieved. For an fcc CoNiCrFeMn alloy it was found that relatively small diffusion barrier difference between interstitials and vacancies contributed to lower defect accumulation [44]. This viewpoint was also discussed for other fcc alloys, like AlCoCrFeNi [72]. Simulations for CoNiCrFeMn [43,44] have been carried out for an irradiation temperature above 700 K, where diffusion would be significantly higher for some defects than in our 300 K irradiation simulations.

Defect diffusion in alloys is complex [21,24], often including sluggish [23] and chemically-biased diffusion [22]. In the fcc HEA studied here, the dumbbell interstitials would have diffusivities which are likely quite different from interstitial diffusivity in pure metals, with the added complexity that the dumbbell might have different atom types at a given step, namely, type could mutate during migration. Migration changes will lead to clustering changes, and differences in the evolution with radiation dose and in the resulting mechanical properties. Regarding defect cluster mobility, we notice that dislocation loop migration would be slower in the HEA, where Peierls stresses are between 100 and 150 MPa, while for the AA are between 6 and 42 MPa [47]. This will also affect radiation damage accumulation. Do and Lee [43] suggested that defect clusters were less stable in a HEA, based on 10 kev cascades in CoNiCrFeMn. Given the large fluctuations we obtain in cluster size distributions, a large number of long annealing simulations would have to be carried out to assess this possible effect in CoNiCrFeCu, which is not present in our preliminary annealing simulations in Fig. S9 of the Supplementary Material.

Kinetic Monte Carlo (kMC) simulations of defect evolution, taking into account cluster binding energies [70] and a distribution of migration barriers for the HEA, could be used to follow the long-term evolution of the primary damage and assess the scope of the radiation resistance in HEAs. It can be shown that the presence of dispersion in migration barriers will lead to a net decrease in barriers with respect to a mean value, and future work might explore how HEA composition would modify values for the mean barrier and its dispersion.

In summary, we presented computer simulation results for a quinary HEA described with empirical Embedded Atom Method potentials. While these model interactions have limitations, they nevertheless represent sensible ways of studying how certain material parameters influence final properties, and therefore guide the design process, provided comparisons are made between materials described by the same potential. Regarding primary radiation damage alone, we can conclude that there is no evidence for radiation resistance in this HEA, and comparison with experiments showing such resistance will require the evaluation of long-term radiation evolution, well beyond the ~0.1 ns simulated in this work. HEA irradiation experiments usually employ high dose MeV irradiation [13,15,17,40], with recent experiments exploring cryogenic temperature irradiation [73,74]. Future studies using instead low dose keV irradiation at cryogenic temperatures, together with high resolution TEM, might be able to aid reaching deeper understanding and model validation for primary damage.

Declaration of Competing Interest

The authors declare that they have no known competing financial interests or personal relationships that could have appeared to influence the work reported in this paper.

Acknowledgements

OD and EMB thank funding from SIIP-UNCuyo grant 06/M104. This work used the Toko cluster from FCEN-UNCuyo, which is part of the SNCAD-MinCyT, Argentina. FV thank the support the Financiamiento Basal para Centros Científicos y Tecnológicos de Excelencia AFB180001, and the Fondo Nacional de Investigaciones Científicas y Tecnológicas (FONDECYT, Chile) under grants #1190662 and #11190484. This research was partially supported by the supercomputing infrastructure of the NLHPC (ECM-02).

Supplementary materials

Supplementary material associated with this article can be found, in the online version, at doi:10.1016/j.actamat.2021.116951.

References

[1] S.J Zinkle, G.S. Was, Materials challenges in nuclear energy, Acta Mater. 61 (2013) 735–758, doi:10.1016/j.actamat.2012.11.004.
[2] ... K. Nordlund, S.J Zinkle, A.E. Sand, F. Granberg, R.S. Averback, R.E. Stoller, F. Willaime, Primary radiation damage: a review of current understanding and models, J. Nucl. Mater. 512 (2018) 450–479, doi:10.1016/j.jnucmat.2018.10.027.
[3] K. Nordlund, S.J Zinkle, A.E. Sand, F. Granberg, R.S. Averback, R.E. Stoller, F. Willaime, Improving atomic displacement and replacement calculations with physically realistic damage models, Nature Commun. 9 (2018) 1–8, doi:10.1038/s41467-018-03415-5.
[4] R.E. Stoller, et al., Primary radiation damage formation, in: R.J.M. Konings, T.R. Allen, R.E. Stoller, S. Yamanaka (Eds.), Comprehensive Nuclear Materials, Elsevier, Amsterdam, 2012, pp. 293–332, doi:10.1016/b978-0-08-056033-5.00027-6.
[5] D.B. Miracle, O.N. Senkov, A critical review of High Entropy Alloys and related concepts, Acta Mater. 122 (2017) 448–511, doi:10.1016/j.actamat.2016.08.081.
[6] Y. Zhou, D. Zhou, X. Jin, L. Zhang, X. Du, B. Li, Design of non-equiatomic medium-entropy alloys, Scient. Rep. 8 (2018) 1–9, doi:10.1038/s41598-018-19449-0.
[7] B.S. Murty, High-Entropy Alloys, Elsevier, 2019.
[8] Z. Li, S. Zhao, R.O. Ritchie, M.A. Meyers, Mechanical properties of high-entropy alloys with emphasis on face-centered cubic alloys, Progr. Mater. Sci. 102 (2019) 296–345, doi:10.1016/j.pmatsci.2018.12.003.
[9] Y. Zhang, T. Zuo, Z. Tang, M.C. Gao, K.A. Dahmen, P.K. Liaw, Z.P. Lu, Microstructures and properties of high-entropy alloys, Progr. Mater. Sci. 61 (2014) 1–93, doi:10.1016/j.pmatsci.2013.10.001.
[10] J. Ding, M. Asta, O. Robert, Melts of CrCoNi-based high-entropy alloys: atomic diffusion and electronic/atomic structure from ab initio simulation, Appl. Phys. Lett. 113 (2018) 111902, doi:10.1063/1.5045216.
[11] B. Gludovatz, A. Hohenwarter, D. Catoor, E. Chang, E.P. George, R.O. Ritchie, A fracture-resistant high-entropy alloy for cryogenic applications, Science 345 (2014) 1153–1158, doi:10.1126/science.1254581.
[12] T. Nagase, P.D. Rack, J.H. Noh, T. Egami, In-situ TEM observation of structural changes in nano-crystalline CoCrCuFeNi multicomponent high-entropy alloy (HEA) under fast electron irradiation by high voltage electron microscopy (HVEM), Intermetallics 59 (2015) 32–42, doi:10.1016/j.intermet.2014.12.007.
[13] Y. Zhang, G.M. Stocks, K. Jin, C. Lu, H. Bei, B.C. Sales, M. Caro, Influence of chemical disorder on energy dissipation and defect evolution in concentrated solid solution alloys, Nat Commun. 6 (2015) 8736, doi:10.1038/ncomms9736.
[14] Y. Zhang, K. Jin, H. Xue, C. Lu, R.J. Olsen, L.K. Beland, G.D. Samolyuk, Influence of chemical disorder on energy dissipation and defect evolution in advanced alloys, J. Mater. Res. 31 (2016) 2363–2375, doi:10.1557/jmr.2016.269.
[15] C. Lu, L. Niu, N. Chen, K. Jin, T. Yang, P. Xiu, M.R. He, Enhancing radiation tolerance by controlling defect mobility and migration pathways in multi-component single-phase alloys, Nature Commun. 7 (2016) 13564, doi:10.1038/ncomms13564.
[16] C. Lu, T. Yang, K. Jin, N. Gao, P. Xiu, Y. Zhang, F. Gao, H. Bei, W.J. Weber, K. Sun, Y. Dong, L. Wang, Radiation-induced segregation on defect clusters in single-phase concentrated solid-solution alloys, Acta Mater. 127 (2017) 98–107, doi:10.1016/j.actamat.2017.01.019.
[17] O. El-Atwani, N. Li, M. Li, A. Devaraj, J.K.S. Baldwin, M.M. Schneider, E. Martinez, Outstanding radiation resistance of tungsten-based high-entropy alloys, Sci. Adv. 5 (2019) eaav2002 https://10.1126/sciadv.aav2002.
[18] F. Wang, X. Yan, T. Wang, Y. Wu, L. Shao, M. Nastasi, B. Cui, Irradiation damage in (Zr0. 25Ta0. 25Nb0. 25Ti0. 25) C high-entropy carbide ceramics, Acta Mater. 195 (2020) 739–749, doi:10.1016/j.actamat.2020.06.011.
[19] M. Caro, L.K Béland, G.D. Samolyuk, R.E. Stoller, A. Caro, Lattice thermal conductivity of multi-component alloys, J. Alloys Comp. 648 (2015) 408–413, doi:10.1016/j.jallcom.2015.06.035.
[20] Y. Lin, T. Yang, L. Lang, C. Shan, H. Deng, W. Hu, F. Gao, Enhanced Radiation Tolerance of the Ni-Co-Cr-Fe high-entropy alloy as revealed from primary damage, Acta Mater. 196 (2020) 133–143, doi:10.1016/j.actamat.2020.06.027.
[21] G. Bonny, D. Chakraborty, S. Pandey, A. Manzoor, N. Castin, S.R. Phillpot, D.S. Aidhy, Classical interatomic potential for quaternary Ni–Fe–Cr–Pd solid solution alloys, Model. Simulat. Mater. Sci. Eng. 26 (2018) 065014, doi:10.1088/1361-651X/aad2e7.
[22] Y. Osetsky, A.V. Barashev, L.K. Béland, Z. Yao, K. Ferasat, Y. Zhang, Tunable chemical complexity to control atomic diffusion in alloys, NPJ Comput. Mater. 6 (2020) 1–8, doi:10.1038/s41524-020-0306-9.
[23] Y.N. Osetsky, L.K. Béland, A.V. Barashev, Y. Zhang, On the existence and origin of sluggish diffusion in chemically disordered concentrated alloys, Curr. Opin. Solid State Mater. Sci. 22 (2018) 65–74, doi:10.1016/j.cossms.2018.05.003.
[24] J. Dąbrowa, D. Marek, State-of-the-art diffusion studies in the high entropy alloys, Metals 10 (2020) 347, doi:10.3390/met10030347.
[25] D. Utt, S. Lee, A. Stukowski, S.H. Oh, G. Dehm, K. Albe, Jerky motion of dislocations in high-entropy alloys: The linkage between local Peierls stress fluctuations and dislocation mobility, https://arxiv.org/abs/2007.11489.
[26] S. Shi, H. Bei, I. Robertson, Impact of alloy composition on one-dimensional glide of small dislocations loops in concentrated solid solution alloys, Mat. Sci Eng. A 700 (2017) 617 https://www.osti.gov/servlets/purl/1366401, doi:10.1016/j.msea.2017.05.049.
[27] M. Robinson, N.A. Marks, G.R. Lumpkin, Sensitivity of the threshold displacement energy to temperature and time, Phys. Rev. B 86 (2012) 134105, doi:10.1103/PhysRevB.86.134105.
[28] A.V. Korchuganov, V.M. Chernov, K.P. Zolnikov, D.S. Kryzhevich, S.G Psakhie, MD simulation of primary radiation damage in metals with internal structure, Inorganic Mater. Appl. Res. 7 (2016) 648–657, doi:10.1134/S2075113316050129.
[29] C. Becquart, A. De Backer, C. Domain, et al., Atomistic modeling of radiation damage in metallic alloys, in: C.-H. Hsueh, et al. (Eds.), Handbook of Mechanics of Materials, Springer Nature Singapore Pte Ltd, 2018, doi:10.1007/978-981-10-6855-3_21-1.
[30] A. Shiryaev, Ion implantation in nanodiamonds: size effect and energy dependence, Scient. Rep. 8 (2018) 1–9, doi:10.1038/s41598-018-23434-y.
[31] D.J. Bacon, F. Gao, Y.N. Osetsky, The primary damage state in fcc, bcc and hcp metals as seen in molecular dynamics simulations, J. Nuclear Mater. 276 (2000) 1–12, doi:10.1016/S0022-3115(99)00165-8.
[32] K. Vörtler, N. Juslin, G. Bonny, L. Malerba, K. Nordlund, The effect of prolonged irradiation on defect production and ordering in Fe–Cr and Fe–Ni alloys, J. Phys. Condensed Matter 23 (2011) 355007, doi:10.1088/0953-8984/23/35/355007.
[33] L.K. Beland, C. Lu, Y.N. Osetsky, G.D. Samolyuk, A. Caro, L. Wang, R.E. Stoller, Features of primary damage by high energy displacement cascades in concentrated Ni-based alloys, J. Appl. Phys. 119 (2016) 085901, doi:10.1063/1.4942533.
[34] L.K. Beland, G.D. Samolyuk, R.E. Stoller, Differences in the accumulation of ion-beam damage in Ni and NiFe explained by atomistic simulations, J. Alloy Comp. 662 (2016) 415–420, doi:10.1016/j.jallcom.2015.11.185.
[35] F. Granberg, K. Nordlund, M.W. Ullah, K. Jin, C. Lu, H. Bei, L. Wang, F. Djurabekova, W. Weber, Y. Zhang, Mechanism of radiation damage reduction in equiatomic multicomponent single phase alloys, Phys. Rev. Lett. 116 (2016) 135504, doi:10.1103/PhysRevLett.116.135504.
[36] C. Shan, L. Lang, T. Yang, Y. Lin, F. Gao, H. Deng, W. Hu, Molecular dynamics simulations of radiation damage generation and dislocation loop evolution in Ni and binary Ni-based alloys, Comput. Mater. Sci. 177 (2020) 109555, doi:10.1016/j.commatsci.2020.109555.
[37] L.K. Béland, Y.N. Osetsky, R.E. Stoller, Atomistic material behavior at extreme pressures, NPJ Comput. Mater. 2 (2016) 16007 085901, doi:10.1038/npjcompumats.2016.7.
[38] M.W. Ullah, H. Xue, G. Velisa, K. Jin, H. Bei, W.J. Weber, Y. Zhang, Effects of chemical alternation on damage accumulation in concentrated solid-solution alloys, Scient. Rep. 7 (2017) 1–11, doi:10.1038/s41598-017-04541-8.
[39] E. Levo, F. Granberg, C. Fridlund, K. Nordlund, F. Djurabekova, Radiation damage buildup and dislocation evolution in Ni and equiatomic multicomponent Ni-based alloys, J. Nuclear Mater. 490 (2017) 323–332, doi:10.1016/j.jnucmat.2017.04.023.
[40] E. Zarkadoula, G. Samolyuk, W.J. Weber, Two-temperature model in molecular dynamics simulations of cascades in Ni-based alloys, J. Alloy Comp. 700 (2017) 106–112, doi:10.1016/j.jallcom.2016.12.441.
[41] F. Tuomisto, Segregation of Ni at early stages of radiation damage in NiCoFeCr solid solution alloys, Acta Mater. 196 (2020) 44–51, doi:10.1016/j.actamat.2020.06.024.
[42] L. Koch, F. Granberg, T. Brink, D. Utt, K. Albe, F. Djurabekova, K. Nordlund, Local segregation versus irradiation effects in high-entropy alloys: Steady-state conditions in a driven system, J. Appl. Phys. 122 (2017) 105106, doi:10.1063/1.4990950.
[43] H.S. Do, B.J. Lee, Origin of radiation resistance in multi-principal element alloys, Scient. Rep. 8 (2018) 1–9, doi:10.1038/s41598-018-34486-5.
[44] Y. Li, R. Li, O. Shigenobu, Reduction of dislocation, mean free path, and migration barriers by High Entropy Alloy: insights from atomistic study of irradiation damage of CoNiCrFeMn, Nanotechnology 31 (2020) 425701, doi:10.1088/1361-6528/ab9cf5.
[45] Y. Li, R. Li, Q. Peng, Enhanced surface bombardment resistance of theCoNiCrFeMn High Entropy Alloy under extreme irradiation flux, Nanotechnology 31 (2020) 025703, doi:10.1088/1361-6528/ab473f.
[46] J.F. Ziegler, J.P. Biersack, U.F. Littmark, The Stopping and Range of ions in Solids. Vol.1 in of Stopping and Ranges of Ions in Matter, Pergamon, New York, 1984.
[47] C. Varvenne, A. Luque, W.G. Nöhring, W.A. Curtin, Average-atom interatomic potential for random alloys, Phys. Rev. B 93 (2016) 104201, doi:10.1103/PhysRevB.93.104201.
[48] R. Pasianot, D. Farkas, Atomistic modeling of dislocations in a random quinary high-entropy alloy, Comput. Mater. Sci. 173 (2020) 109366, doi:10.1016/j.commatsci.2019.109366.

[49] D. Farkas, Grain boundary structure in high-entropy alloys, J. Mater. Sci. 55 (2020) 1–11, doi:10.1007/s10853-020-04387-y.
[50] D. Farkas, A. Caro, Model interatomic potentials and lattice strain in a high-entropy alloy, J. Mat. Res. 33 (2018) 3218–3225, doi:10.1557/jmr.2018.245.
[51] S. Plimpton, Fast parallel algorithms for short-range molecular dynamics, J. Comput. Phys. 117 (1995) 1–19, doi:10.1006/jcph.1995.1039.
[52] A. Stukowski, Visualization and analysis of atomistic simulation data with OVITO: the open visualization tool, Model. Simulat. Mater. Sci. Eng. 18 (2010) 015012, doi:10.1088/0965-0393/18/1/015012.
[53] A. Stukowski, Structure identification methods for atomistic simulations of crystalline materials, Model. Simulat. Mater. Sci. Eng. 20 (2012) 045021, doi:10.1088/0965-0393/20/4/045021.
[54] A. Stukowski, Computational analysis methods in atomistic modeling of crystals, JOM 66 (2014) 399–407, doi:10.1007/s11837-013-0827-5.
[55] P.M Larsen, S. Schmidt, J. Schiøtz, Robust structural identification via polyhedral template matching, Model. Simulat. Mater. Sci. Eng. 24 (2016) 055007, doi:10.1088/0965-0393/24/5/055007.
[56] J. Lindhard, M. Scharff, Energy dissipation by ions in the keV region, Phys. Rev. 124 (1961) 128, doi:10.1103/PhysRev.124.128.
[57] A. Caro, M. Victoria, Ion-electron interaction in molecular-dynamics cascades, Phys. Rev. A 40 (1989) 2287–2291, doi:10.1103/PhysRevA.40.2287.
[58] K. Nordlund, M. Ghaly, R.S. Averback, M. Caturla, D.T. Rubia, J. Tarus, Defect production in collision cascades in elemental semiconductors and fcc metals, Phys. Rev. B 57 (1998) 7556, doi:10.1103/PhysRevB.57.7556.
[59] D.M. Duffy, A.M. Rutherford, Including the effects of electronic stopping and electron–ion interactions in radiation damage simulations, J. Phys. Condensed Matter 19 (2006) 016207, doi:10.1088/0953-8984/19/1/016207.
[60] H. Hemani, A. Majalee, U. Bhardwaj, A. Arya, K. Nordlund, M. Warrier, Inclusion and validation of electronic stopping in the open source LAMMPS code, https://arxiv.org/abs/2005.11940v1.
[61] E. Quashie, R. Ullah, X. Andrade, A.A. Correa, Effect of chemical disorder on the electronic stopping of solid solution alloys, Acta Mater. 196 (2020) 576–583, doi:10.1016/j.actamat.2020.06.061.
[62] J. Ziegler, The stopping and range of ions in matter; http://www.SRIM.org.
[63] D.I. Thwaites, Bragg's rule of stopping power additivity: A compilation and summary of results, Radiat. Res. 95 (1983) 495–518, doi:10.2307/3576096.
[64] S. Zhao, Y. Osetsky, A.V. Barashev, Y. Zhang, Frenkel defect recombination in Ni and Ni–containing concentrated solid–solution alloys, Acta Mater. 173 (2019) 184–194, doi:10.1016/j.actamat.2019.04.060.
[65] Z. Yao, M.J Caturla, R. Schäublin, Study of cascades damage in Ni by MD with different interatomic potentials, J. Nuclear Mater. 367 (2007) 298–304, doi:10.1016/j.jnucmat.2007.03.136.
[66] M.A. Cusentino, M.A. Wood, R. Dingreville, Compositional and structural origins of radiation damage mitigation in high-entropy alloys, J. Appl. Phys. 128 (2020) 125904, doi:10.1063/5.0024014.
[67] M.J. Norgett, M.T. Robinson, I.M. Torrens, A proposed method of calculating displacement dose rates, Nuclear Eng. Des. 33 (1975) 50–54, doi:10.1016/0029-5493(75)90035-7.
[68] A.Y. Konobeyev, U. Fischer, Y.A. Korovin, S.P. Simakov, Evaluation of effective threshold displacement energies and other data required for the calculation of advanced atomic displacement cross-sections, Nuclear Energy Technol. 3 (2017) 169–175, doi:10.1016/j.nucet.2017.08.007.
[69] C. Lu, L. Niu, N. Chen, K. Jin, T. Yang, P. Xiu, Y. Zhang, F. Gao, H. Bei, S. Shi, M.-R. He, I.M. Robertson, W.J. Weber, L. Wang, Enhancing radiation tolerance by controlling defect mobility and migration pathways in multicomponent single-phase alloys, Nature Commun. 7 (2016) 13564 https://www.nature.com/articles/ncomms13564.
[70] G. Arora, G. Bonny, N. Castin, D.S. Aidhy, Effect of different point-defect energetics in $Ni_{80}X_{20}$ (X=Fe, Pd) on contrasting vacancy cluster formation from atomistic simulations, Acta Mat. 15 (2021) 100974, doi:10.1016/j.mtla.2020.100974.
[71] L.K. Béland, Y.N. Osetsky, R.E. Stoller, The effect of alloying nickel with iron on the supersonic ballistic stage of high energy displacement cascades, Acta Mat. 116 (2016) 136–142, doi:10.1016/j.actamat.2016.06.031.
[72] T. Yang, S. Xia, S. Liu, C. Wang, S. Liu, Y. Fang, Y. Wang, Precipitation behavior of Al_xCoCrFeNi High Entropy Alloys under ion irradiation, Scient. Rep. 6 (2016) 32146, doi:10.1038/srep32146.
[73] C. Parkin, M. Moorehead, M. Elbakhshwan, J. Hu, W.Y. Chen, M. Li, A. Couet, *In situ* microstructural evolution in face-centered and body-centered cubic complex concentrated solid-solution alloys under heavy ion irradiation, Acta Mater. 198 (2020) 85–99, doi:10.1016/j.actamat.2020.07.066.
[74] C. Mieszczynski, R. Ratajczak, J. Jagielski, G. Velişa, H. Bei, B.C Sales, Y. Zhang, Defect evolution in Ni and solid-solution alloys of NiFe and NiFeCoCr under ion irradiation at 16 and 300 K, J. Nuclear Mater. 534 (2020) 152138, doi:10.1016/j.jnucmat.2020.152138.